Strain fields in InAs/GaAs quantum wire structures: Inclusion versus inhomogeneity

E. Pan[a] and F. Han
University of Akron, Akron, Ohio 44039

J. D. Albrecht
Air Force Research Laboratory, Wright-Patterson Air Force Base, Ohio 45433

(Received 29 November 2004; accepted 15 May 2005; published online 12 July 2005)

This paper studies the elastic fields in InAs/GaAs quantum wire (QWR) structures arising from the lattice mismatch between InAs and GaAs. The present treatment is different from recent analyses based on the Eshelby inclusion approach where the QWR material, for simplicity, is assumed to be the same as the matrix/substrate. Here, a more complete treatment is developed taking into account the structural inhomogeneity using the boundary integral equation method. We implement our model using discrete boundary elements at the interface between the QWR and its surrounding matrix. The coefficients of the algebraic equations are derived exactly for constant elements using our recent Green's-function solutions in the Stroh formalism. For both (001) and (111) growth directions, our results show that while the elastic fields far from the QWR are approximated well by the homogeneous inclusion approach, for points within or close to the QWR, the differences between the fields computed with the simplified inclusion and complete inhomogeneity models can be as large as 10% for the test system. These differences in the strain fields will have strong implications for the modeling of the quantized energy states of the quantum wire nanostructures. Since the strain fields inside and close to the wire are more important than the exterior strain fields from the standpoint of the confined electronic states, we suggest that in the vicinity of the QWR, the inhomogeneity model be used with proper elastic constants, while the simple exact inclusion model be used in the bulk of surrounding medium. © *2005 American Institute of Physics*.
[DOI: 10.1063/1.1948510]

I. INTRODUCTION

Quantum wire (QWR) semiconductor nanostructures and their quantum-mechanical properties have been the subjects of many investigations over the past decade.[1–5] Similar to quantum-dot (QD) structures, the electronic energy features are closely related to and in some cases can be controlled by the strain field induced by the lattice and/or thermal mismatches among component materials. As a first approximation to fabricated structures, the intrinsic material differences (mostly the differences in elastic compliances) between the QWR/QD and its substrate were ignored.[6–8] The crucial simplification of these approaches is to impose a strain field arising from lattice mismatches without allowing for variations in the material constants from material to material. This approximation was recently shown to be reliable for computing the strain fields sufficiently away from the QWR where the system is sensitive to the QWR geometry and interfacial mismatch, but relatively unaffected by the internal properties of the QWR.[9–11] Whether this approximation is valid for points inside and close to the QWR (the crucial locations from an electronic device standpoint) is suspect and is the motivation for the present investigation.

In previous treatments, many researchers use the established Eshelby inclusion method[12,13] to solve the QWR-induced field. By convention, the so-called Eshelby inclusion problem is that of an embedded subdomain, such as a QWR, consisting of a material which is modeled as a strained region but with identical mechanical properties as the matrix (i.e., substrate, buffer, or overgrowth layers). We contrast this with the structural inhomogeneity problem where the materials are different in all respects except for their lattice type.[13] Investigations of homogeneous polygonal inclusions have been carried out for both isotropic and anisotropic elastic cases.[11,14–16] More recently, general solutions to anisotropic Eshelby problems that account for electromechanical coupling have been derived. These solutions are based either on the analytical continuation and conformal mapping method[10,17,18] or on the Green's-function method using the equivalent body-force concept.[19,20] Numerically, the finite element method (FEM) and finite difference method (FDM) have been successfully applied to the strained QD or QWR problems,[1,21,22] and so has the boundary integral equation method [i.e., the boundary element method (BEM)] with its advantages in dealing with singularities and comparatively smaller computational demands.[23,24]

In this paper, we address the issue of homogeneous inclusion versus structural inhomogeneity in the context of QWR semiconductor structures. The model is based on the formalism recently proposed by one of the authors[19] and treated computationally using an accurate BEM. First, we convert the contribution of the eigenstrain to an integral along the interface of the QWR and its matrix/substrate. After this conversion, the boundary integral equation is applied

[a]Electronic mail: pan2@uakron.edu

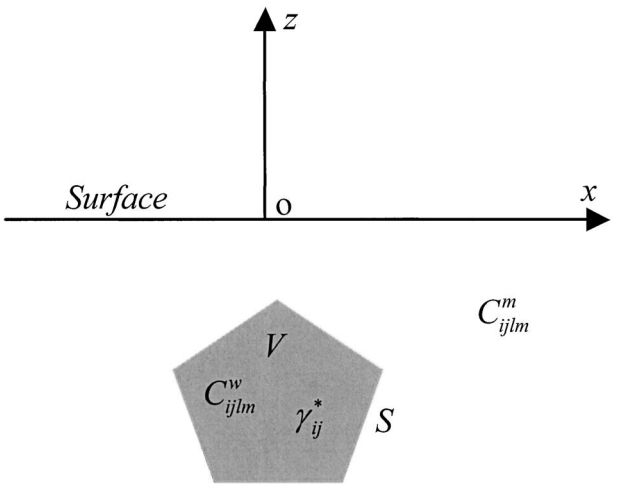

FIG. 1. An arbitrarily shaped polygon QWR inclusion/inhomogeneity in an anisotropic (x,z) half plane $(z<0)$: An eigenstrain γ^*_{ij} within the QWR.

to both the QWR and substrate. Using constant-element discretization, the integration of the Green's function is carried out exactly and the resulting system of algebraic equations is solved for the interface quantities. The elastic fields inside and outside the QWR are subsequently evaluated using the solved interfacial values.

As numerical examples, InAs/GaAs QWR structures are analyzed for both (001) and (111) growth directions. QWRs with square and trapezoidal cross sections are considered. The results of this work show several features which should be useful for numerical modeling when accounting for strain fields in device designs: (i) In the substrate and far away from the QWR, both the inclusion and inhomogeneity models give similar results. In other words, we have validated that if one is only interested in the elastic far fields, the simplified homogeneous inclusion model can be safely applied. (ii) For points within or near the QWR, the difference between the inclusion and inhomogeneity models can be as high as 10% for these materials. Using a linear band-gap deformation potential relation, this could correspond to a substantial modification of the local electronic energy band gap. (iii) Although the singular behavior near the corners of the QWR looks similar for both the homogeneous inclusion and the structural inhomogeneity models, the amplitudes of the singularity are different, giving rise to potentially strong deviations from the simplified models depending on the materials and geometries.

II. PROBLEM DESCRIPTION AND BASIC EQUATIONS

Let us suppose that there is a misfit elastic strain γ^*_{ij} $(i,j=1,2,3)$ inside an arbitrarily shaped polygon QWR domain V, which is embedded in the $z<0$ half plane substrate as shown in Fig. 1. Assume also that the misfit strain is uniform within the QWR and is zero outside. The interface between the QWR and matrix is labeled S. We also denote C^w_{ijkl} and C^m_{ijkl} as the elastic moduli of the QWR and the matrix materials, respectively. For the homogeneous inclusion problem, $C^w_{ijkl}=C^m_{ijkl}$.

We define γ_{ij} as the total elastic strain, which is related to the total elastic displacement u_i as

$$\gamma_{ij}=(u_{i,j}+u_{j,i})/2. \tag{1}$$

The total strain can be written as

$$\gamma_{ij}=\gamma^e_{ij}+\gamma^*_{ij}, \tag{2}$$

where γ^e_{ij} is the elastic strain that appears in the constitutive relation

$$\sigma_{ij}=C_{ijkl}\gamma^e_{kl}, \tag{3}$$

which can be written as

$$\sigma_{ij}=C_{ijkl}(\gamma_{kl}-\chi\gamma^*_{kl}). \tag{4}$$

In Eq. (4), χ is equal to one if the field point is within the QWR domain V and zero in the substrate. σ_{ij} is the stress and C_{ijkl} is the material elastic modulus, replaced with either C^w_{ijkl} or C^m_{ijkl} depending on the problem domain. We further define the traction

$$t_i=\sigma_{ji}n_j \quad (i,j=1,2,3), \tag{5}$$

where n_j are the direction cosines of the outward normal $\boldsymbol{n}$ along the interface S.

Substituting the stress in Eq. (4) into the equilibrium equation for the stress

$$\sigma_{ij,i}+f_j=0 \tag{6}$$

results in the expression

$$C^w_{ijkl}u_{k,li}-C^w_{ijkl}\gamma^*_{kl,i}=0 \tag{7}$$

for the QWR domain. It is clear that the second term in Eq. (7) is equivalent to a body force defined as

$$f^{(w)}_j=-C^w_{ijkl}\gamma^*_{kl,i}, \tag{8}$$

which is also called the equivalent body force of the eigenstrain.[13,19] This equivalent body force will be employed in Sec. III to convert the contribution of the eigenstrain to a boundary integral along the interface of the QWR and its substrate.

III. BOUNDARY INTEGRATION EQUATIONS AND CONSTANT-ELEMENT DISCRETIZATION

To solve the problem in Fig. 1, we apply the BEM to both the QWR and its matrix/substrate. The boundary integral formulation can be derived with the result that[23]

$$b_{ij}(\mathbf{X})u^{(m)}_j(\mathbf{X})=\int_S [U^{(m)}_{ij}(\mathbf{X},\mathbf{x})t^{(m)}_j(\mathbf{x}) - T^{(m)}_{ij}(\mathbf{X},\mathbf{x})u^{(m)}_j(\mathbf{x})]dS(\mathbf{x}) \tag{9}$$

for the matrix, and

$$b_{ij}(\mathbf{X})u^{(w)}_j(\mathbf{X})=\int_S \{U^{(w)}_{ij}(\mathbf{X},\mathbf{x})[t^{(w)}_j(\mathbf{x})+f^{(w)}_j(\mathbf{x})] - T^{(w)}_{ij}(\mathbf{X},\mathbf{x})u^{(w)}_j(\mathbf{x})\}dS(\mathbf{x}) \tag{10}$$

for the QWR. The superscripts (m) and (w) denote quantities associated with the matrix and wire, respectively.

In Eqs. (9) and (10) t_j and u_j are the traction and displacement components, and $\boldsymbol{x}$ and $\boldsymbol{X}$ are the coordinates of the field and source points, respectively. The coefficient b_{ij} is equal to δ_{ij} if $\boldsymbol{X}$ is an interior point and $(1/2)\delta_{ij}$ at a smooth boundary point. For points at complicated geometric locations, these coefficients can be determined by the rigid-body motion method.[23] Furthermore, in Eq. (10), $f_j^{(w)}$ is the traction induced by the misfit elastic eigenstrain inside the QWR, which is given by Eq. (8).

The Green's functions U_{ij} and T_{ij} in Eqs. (9) and (10) are taken to be the special two-dimensional Green's functions for full/half plane, which are described in detail in Ref. 19. The indices i and j indicate the jth Green's elastic displacement/traction (at $\boldsymbol{x}$) in response to a line force in the ith direction (applied at $\boldsymbol{X}$). For the sake of easy reference, we will briefly present the general results with the definitions for the involved physical quantities appearing in subsequent sections. Note also that the Green's functions[19] are in exact closed form, and thus their integration over constant elements can be carried out exactly as detailed in Sec. IV. This is computationally desirable as it is very efficient and accurate for the simulation.

Employing constant-value elements, we divide the boundary (interface) into N segments with the nth element being labeled as Γ_n. The constant values u_{jn} and t_{jn} on the nth element equal to those at the center of the element. Under this assumption, the boundary integral equations (9) and (10) for the surrounding matrix and QWR domains are reduced to the following algebraic equations:

$$b_{ij}u_j + \sum_{n=1}^{N}\left(\int_{\Gamma_n} T_{ij}^{(m)} d\Gamma\right)u_{jn} = \sum_{n=1}^{N}\left(\int_{\Gamma_n} U_{ij}^{(m)} d\Gamma\right)t_{jn} \tag{11}$$

and

$$b_{ij}u_j + \sum_{n=1}^{N}\left(\int_{\Gamma_n} T_{ij}^{(w)} d\Gamma\right)u_{jn} = \sum_{n=1}^{N}\left(\int_{\Gamma_n} U_{ij}^{(m)} d\Gamma\right) \times (t_{jn} + C_{ijkl}^{(w)}\gamma_{kl}^{*}n_j). \tag{12}$$

Obviously, the difference between Eqs. (11) and (12) is that there is a traction induced by the misfit elastic eigenstrain inside the QWR in Eq. (12).

Given the central Eqs. (11) and (12), the problem now is to find the suitable Green's functions U_{ij} and T_{ij}, as well as their integrals on each element Γ_n, which are the kernel functions in these equations. In Secs. V and VI, we will concentrate on the derivation of the Green's displacement and its integral, because all the other physical quantities, such as the strain, stress, etc., can be derived uniquely from the displacement.

IV. ELASTIC HALF PLANE GREEN'S FUNCTION

We consider an anisotropic half plane with its surface at $z=0$ and the half plane occupies the $z<0$ domain, as in Fig. 1. We assume that the deformation is independent of the y coordinate [i.e., the generalized plane strain deformation in the (x,z) plane]. This means that the lattice mismatch would also be present along y but extends to infinity in the y direction. In this paper, we assume that the half plane surface is traction-free. We further let a line force $\boldsymbol{f}=(f_1,f_2,f_3)$ be applied at (X,Z) with $Z<0$.

First, the expression of displacement Green's-function matrix $\boldsymbol{U}$ (i.e., U_{ij}) is derived from the Stroh formalism. Using the basic Eqs. (1)–(5), the traction Green's-function matrix $\boldsymbol{T}$ can be derived from $\boldsymbol{U}$. It can be shown[12,25] that the half plane displacement Green's functions can be expressed as

$$\boldsymbol{U} = \frac{1}{\pi}\,\mathrm{Im}\{\boldsymbol{A}\langle \ln(z_* - s_*)\rangle \boldsymbol{A}^T\} + \frac{1}{\pi}\,\mathrm{Im}\sum_{j=1}^{3}\{\boldsymbol{A}\langle \ln(z_* - \bar{s}_j)\rangle \boldsymbol{Q}_j\}. \tag{13}$$

In Eq. (13), Im stands for the imaginary part of a complex variable, and p_j [contained in z_* and s_* as shown in Eqs. (14)–(16) below] and $\boldsymbol{A}$ are the Stroh eigenvalues and the corresponding eigenmatrices with their expressions given in Appendix A. Finally in Eq. (13),

$$\langle \ln(z_* - s_*)\rangle = \mathrm{diag}[\ln(z_1 - s_1), \ln(z_2 - s_2), \ln(z_3 - z_3)], \tag{14}$$

where the complex variables z_j and s_j $(j=1,2,3)$ are defined, respectively, by

$$z_j = x + p_j z \tag{15}$$

and

$$s_j = X + p_j Z. \tag{16}$$

It is further noticed that the first term in Eq. (13) corresponds to the full-plane Green's function and the second term in Eq. (13) is the complementary part of the solution with the complex constant matrices $\boldsymbol{Q}_j$ $(j=1,2,3)$ being determined as

$$\boldsymbol{Q}_j = \boldsymbol{B}^{-1}\bar{\boldsymbol{B}}\boldsymbol{I}_j\bar{\boldsymbol{A}}^T, \tag{17}$$

where the complex matrix $\boldsymbol{B}$ is an eigenmatrix defined in Appendix A, and the diagonal matrices $\boldsymbol{I}_j$ $(j=1,2,3)$ have the form

$$\boldsymbol{I}_1 = \mathrm{diag}[1,0,0], \quad \boldsymbol{I}_2 = \mathrm{diag}[0,1,0], \quad \boldsymbol{I}_3 = \mathrm{diag}[0,0,1]. \tag{18}$$

With the displacement Green's-function matrix given by Eq. (13), its derivatives with respect to the field and source points can be carried out analytically and the resulting Green's-function derivatives can then be applied to various

problems associated with a half plane under traction-free boundary conditions. In Sec. V we derive the exact boundary integral for these Green's functions by assuming that the interface between the QWR and its matrix is made of piecewise straight-line segments with constant field quantities on each segment.

V. ANALYTICAL INTEGRATION OF KERNEL FUNCTIONS AND REDUCED ALGEBRAIC EQUATIONS

To carry out the line integral of the Green's functions, we first write Eq. (13) in terms of the matrix components, i.e.,

$$U_{ij}(\boldsymbol{x},\boldsymbol{X}) = \frac{1}{\pi}\,\mathrm{Im}\{A_{jr}\ln(z_r - s_r)A_{ir}\} + \frac{1}{\pi}\,\mathrm{Im}\sum_{v=1}^{3}\{A_{jr}\ln(z_r - \bar{s}_v)Q_{ri}^{v}\}, \tag{19}$$

where the repeated index r takes the summation from 1 to 3, and

$$Q_{ri}^{v} = B_{rs}^{-1}\bar{B}_{sp}(I_v)_p\bar{A}_{ip}. \tag{20}$$

Next we define a line segment in the (x,z) plane starting from point 1 (x_1,z_1) and ending at point 2 (x_2,z_2), in terms of the parameter t $(0\leqslant t\leqslant 1)$, as

$$x = x_1 + (x_2 - x_1)t, \qquad z = z_1 + (z_2 - z_1)t, \tag{21}$$

so that the outward normal component $n_i(\boldsymbol{x})$ along the line segment is constant, given by

$$n_1 = (z_2 - z_1)/l, \quad n_3 = -(x_2 - x_1)/l, \tag{22}$$

where l is the length of the line segment and the elemental length is $d\Gamma = ldt$.

Note again that the half plane displacement Green's functions consist of two parts: the full-plane Green's function and a complementary part. Therefore, the corresponding integrals in Eqs. (11) and (12) also consist of two parts involving two types of functions. For the first integral, we define

$$h_r(X,Z) \equiv \int_0^1 \ln(z_r - s_r)dt = \int_0^1 \ln\{[(x_2 - x_1) + p_r(z_2 - z_1)]t + [(x_1 + p_r z_1) - s_r]\}dt. \tag{23}$$

Carrying out the integration gives

$$h_r(X,Z) = \frac{(x_1 + p_r z_1) - s_r}{(x_2 - x_1) + p_r(z_2 - z_1)}\ln\left(\frac{x_2 + p_r z_2 - s_r}{x_1 + p_r z_1 - s_r}\right) + \ln(x_2 + p_r z_2 - s_r) - 1. \tag{24}$$

Similarly, we define the second integral as

$$g_r^{v}(X,Z) \equiv \int_0^1 \ln(z_r - \bar{s}_v)dt, \tag{25}$$

and integration of the right-hand side gives

$$g_r^{v}(X,Z) = \frac{(x_1 + p_r z_1) - \bar{s}_v}{(x_2 - x_1) + p_r(z_2 - z_1)}\ln\left(\frac{x_2 + p_r z_2 - \bar{s}_v}{x_1 + p_r z_1 - \bar{s}_v}\right) + \ln(x_2 + p_r z_2 - \bar{s}_v) - 1. \tag{26}$$

Finally, the integral of the displacement Green's function from the contribution of a constant boundary element can be obtained in the closed form as

$$\hat{U}_{ij}(\boldsymbol{X}) = \int_\Gamma U_{ij}(\boldsymbol{x},\boldsymbol{X})d\Gamma = \frac{l}{\pi}\,\mathrm{Im}\left[A_{jr}h_r(X,Z)A_{ir} + \sum_{v=1}^{3}A_{jr}g_r^{v}(X,Z)Q_{ri}^{v}\right]. \tag{27}$$

The first term involving h_r is the contribution from the full-plane Green's function, and the second term involving g_r^{v} comes from the complementary part, which is used to satisfy the boundary conditions on the surface of the half plane.

To find the analytical integration for the traction Green's function, we first write Eq. (19) as

$$U_{ij}(\boldsymbol{x},\boldsymbol{X}) = \frac{1}{\pi}\,\mathrm{Im}[A_{jr}d_r(\boldsymbol{x},\boldsymbol{X})A_{ir}] + \frac{1}{\pi}\,\mathrm{Im}\sum_{v=1}^{3}[A_{jr}e_r^{v}(\boldsymbol{x},\boldsymbol{X})Q_{ri}^{v}], \tag{28}$$

where $d_r(\boldsymbol{x},\boldsymbol{X}) = \ln(z_r - s_r)$ and $e_r^{v}(\boldsymbol{x},\boldsymbol{X}) = \ln(z_r - \bar{s}_v)$. The strain field can be obtained by taking the derivative of Eq. (28) with respect to the field coordinate $\boldsymbol{x} = (x,z)$, as (α, $\beta = 1$ and 3):

$$\gamma_{\alpha\beta}^{j}(\boldsymbol{x},\boldsymbol{X}) = 0.5\frac{1}{(\pi)}\,\mathrm{Im}\left[A_{\alpha r}d_{r,\beta}(\boldsymbol{x},\boldsymbol{X})A_{ir} + \sum_{v=1}^{3}A_{\alpha r}e_{r,\beta}^{v}(\boldsymbol{x},\boldsymbol{X})Q_{ri}^{v}\right] + 0.5\frac{1}{(\pi)}\,\mathrm{Im}\left[A_{\beta r}d_{r,\alpha}(\boldsymbol{x},\boldsymbol{X})A_{ir} + \sum_{v=1}^{3}A_{\beta r}e_{r,\alpha}^{v}(\boldsymbol{x},\boldsymbol{X})Q_{ri}^{v}\right], \tag{29}$$

and

$$\gamma_{2\beta}^{j}(\boldsymbol{x},\boldsymbol{X}) = 0.5\frac{1}{(\pi)}\,\mathrm{Im}\left[A_{2r}d_{r,\beta}(\boldsymbol{x},\boldsymbol{X})A_{ir} + \sum_{v=1}^{3}A_{2r}e_{r,\beta}^{v}(\boldsymbol{x},\boldsymbol{X})Q_{ri}^{v}\right], \tag{30}$$

where

$$d_{r,1}(\boldsymbol{x},\boldsymbol{X}) = \frac{1}{z_r - s_r}, \quad d_{r,3}(\boldsymbol{x},\boldsymbol{X}) = \frac{p_r}{z_r - s_r} \tag{31}$$

and

$$e^{v}_{r,1}(\boldsymbol{x},\boldsymbol{X}) = \frac{1}{z_r - \bar{s}_v}, \quad e^{v}_{r,3}(\boldsymbol{x},\boldsymbol{X}) = \frac{\bar{p}_v}{z_r - \bar{s}_v}. \tag{32}$$

Making use of the constitutive relation in Eq. (3) and the traction expression of Eq. (5), the traction Green's function can be expressed as

$$T_{ij}(\boldsymbol{x},\boldsymbol{X}) = \sigma^{i}_{jk}(\boldsymbol{x},\boldsymbol{X})n_k = C_{jk\alpha\beta}\gamma^{i}_{\alpha\beta}(\boldsymbol{x},\boldsymbol{X})n_k, \tag{33}$$

where the repeated indices k, α, and β take the summation over 1 through 3.

Using Eq. (33), the integral of the traction Green's function from the contribution of a constant boundary element can then be obtained in the closed form as

$$\begin{aligned}\hat{T}_{ij}(\boldsymbol{X}) &= \int_{\Gamma} T_{ij}(\boldsymbol{x},\boldsymbol{X})d\Gamma \\ &= \int_{\Gamma} C_{jk\alpha\beta}\gamma^{i}_{\alpha\beta}(\boldsymbol{x},\boldsymbol{X})n_k d\Gamma \\ &= C_{jk\alpha\beta}\left(\int_{\Gamma} \gamma^{i}_{\alpha\beta}(\boldsymbol{x},\boldsymbol{X})d\Gamma\right)n_k,\end{aligned} \tag{34}$$

where the kernel part, i.e., the integration of the strain field, is

$$\begin{aligned}\int_{\Gamma} \gamma^{i}_{\alpha\beta}(\boldsymbol{x},\boldsymbol{X})d\Gamma = {} & 0.5\frac{l}{(\pi)}\,\mathrm{Im}\left[A_{\alpha r}\hat{d}_{r\beta}(X,Z)A_{ir} + \sum_{v=1}^{3} A_{\alpha r}\hat{e}^{v}_{r\beta}(X,Z)Q^{v}_{ri}\right] \\ & + 0.5\frac{l}{(\pi)}\,\mathrm{Im}\left\{A_{\beta r}\hat{d}_{r\alpha}(X,Z)A_{ir} + \sum_{v=1}^{3} A_{\beta r}\hat{e}^{v}_{r\alpha}(X,Z)Q^{v}_{ri}\right\},\end{aligned} \tag{35}$$

and

$$\begin{aligned}\int_{\Gamma} \gamma^{i}_{2\beta}(\boldsymbol{x},\boldsymbol{X})d\Gamma = {} & 0.5\frac{1}{(\pi)}\,\mathrm{Im}\left\{A_{2r}\hat{d}_{r\beta}(X,Z)A_{ir} + \sum_{v=1}^{3} A_{2r}\hat{e}^{v}_{r\beta}(X,Z)Q^{v}_{ri}\right\},\end{aligned} \tag{36}$$

where

$$\hat{d}_{r1}(X,Z) = \int_0^1 d_{r,1}(\boldsymbol{x},\boldsymbol{X})dt = \frac{1}{(x_2 - x_1) + p_r(z_2 - z_1)}\ln\left(\frac{x_2 + p_r z_2 - s_r}{x_1 + p_r z_1 - s_r}\right), \tag{37}$$

$$\hat{d}_{r3}(X,Z) = \int_0^1 d_{r,3}(\boldsymbol{x},\boldsymbol{X})dt = \frac{p_r}{(x_2 - x_1) + p_r(z_2 - z_1)}\ln\left(\frac{x_2 + p_r z_2 - s_r}{x_1 + p_r z_1 - s_r}\right), \tag{38}$$

$$\hat{e}^{v}_{r1}(X,Z) = \int_0^1 e^{v}_{r,1}(\boldsymbol{x},\boldsymbol{X})dt = \frac{1}{(x_2 - x_1) + p_r(z_2 - z_1)}\ln\left(\frac{x_2 + p_r z_2 - \bar{s}_v}{x_1 + p_r z_1 - \bar{s}_v}\right), \tag{39}$$

and

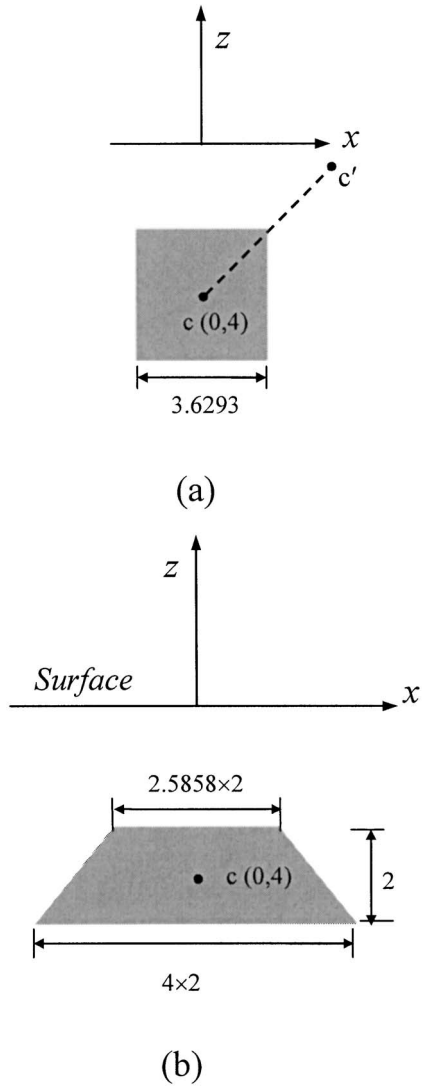

FIG. 2. Cross-section parameters of the QWR buried in GaAs matrix: (a) Square QWR buried in GaAs full plane. (b) A trapezoid QWR buried in GaAs half plane.

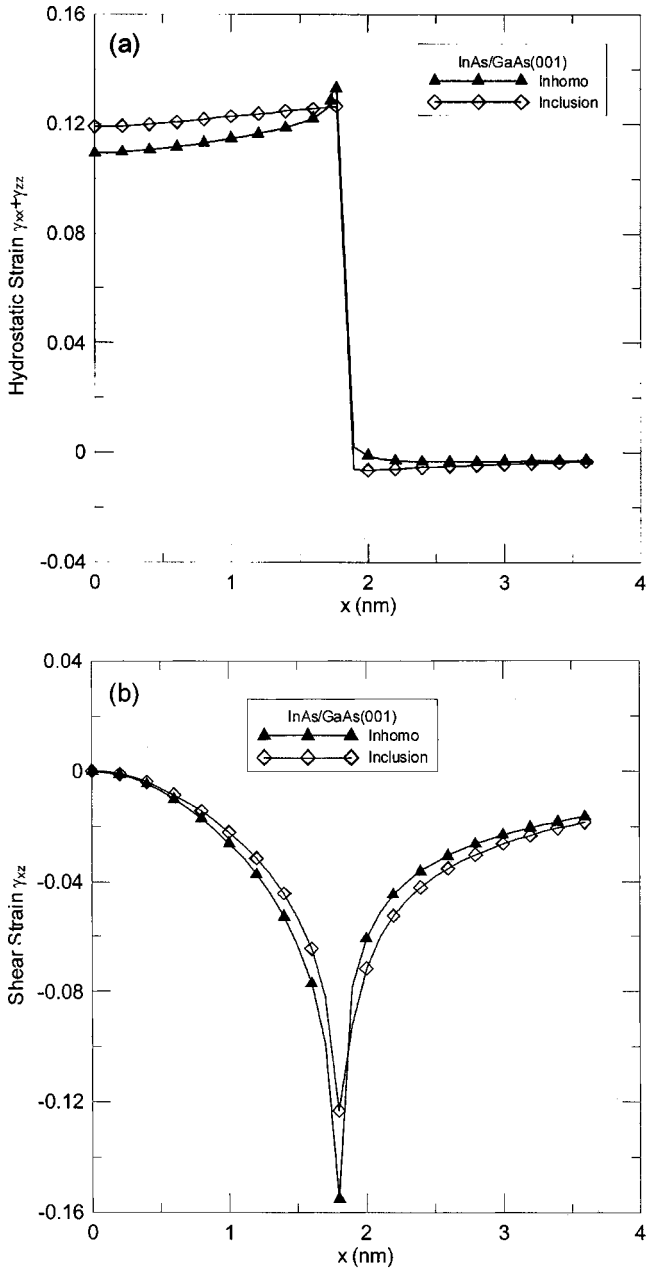

FIG. 3. Variation of strain field along the upper right diagonal line of square QWR inside GaAs (001) matrix: GaAs (001) inclusion vs InAs (001) inhomogeneity. Hydrostatic strain $(\gamma_{xx}+\gamma_{zz})$ in (a), and shear strain γ_{xz} in (b).

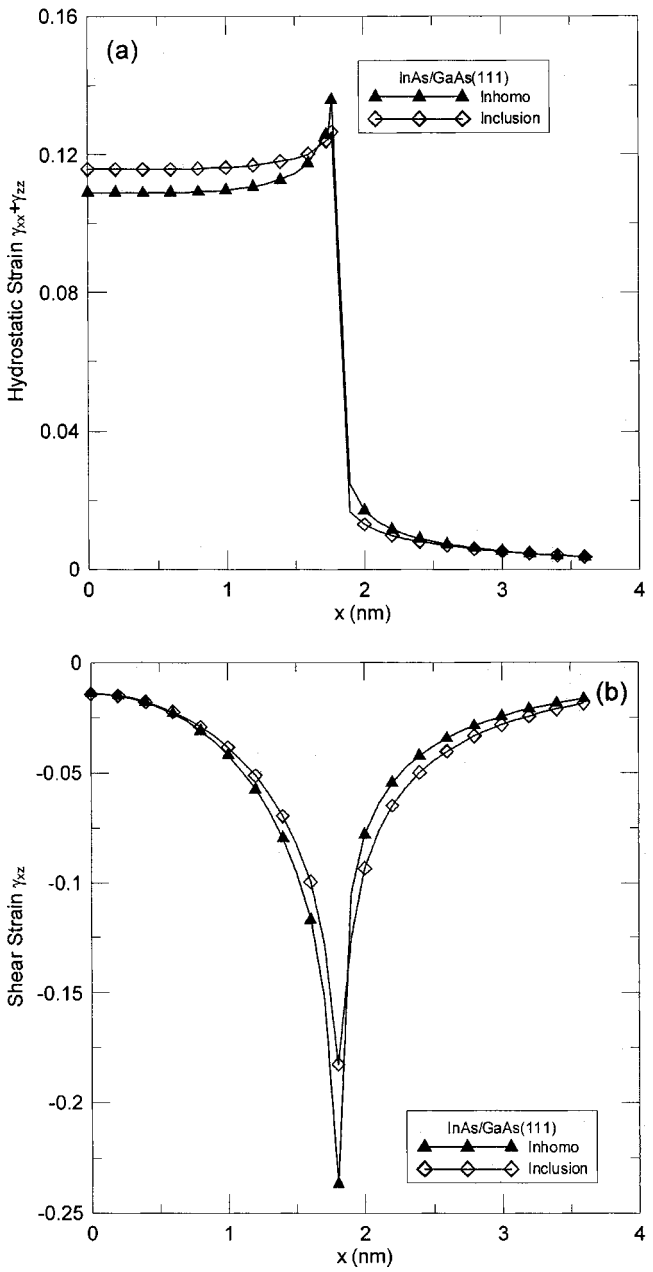

FIG. 4. Variation of strain field along the upper right diagonal line of square QWR inside GaAs (111) matrix: GaAs (111) inclusion vs InAs (111) inhomogeneity. Hydrostatic strain $(\gamma_{xx}+\gamma_{zz})$ in (a), and shear strain γ_{xz} in (b).

$$\hat{e}^{v}_{r3}(X,Z) = \int_0^1 e^{v}_{r,3}(\boldsymbol{x},\boldsymbol{X})dt = \frac{\bar{p}_v}{(x_2-x_1)+p_r(z_2-z_1)} \ln\left(\frac{x_2+p_r z_2-\bar{s}_v}{x_1+p_r z_1-\bar{s}_v}\right). \tag{40}$$

Therefore, using the constant-element discretization the two boundary integral equations (11) and (12) for the QWR and matrix/substrate can be cast into a system of algebraic equations for the interface points. In matrix form, they can be expressed as

$$\hat{\boldsymbol{U}}^{(w)}\boldsymbol{t}^{(w)} - \hat{\boldsymbol{T}}^{(w)}\boldsymbol{u}^{(w)} = \boldsymbol{f}^{(w)}, \tag{41}$$

and

$$\hat{\boldsymbol{U}}^{(m)}\boldsymbol{t}^{(m)} - \hat{\boldsymbol{T}}^{(m)}\boldsymbol{u}^{(m)} = 0, \tag{42}$$

where the coefficients $\hat{\boldsymbol{U}}$ and $\hat{\boldsymbol{T}}$ are the exact integrals of Green's functions on each constant element given in Eqs. (27) and (34), and $\boldsymbol{u}$ and $\boldsymbol{t}$ are the displacement and traction vectors in the center of each constant element. The right-hand-side term $\boldsymbol{f}^{(w)}$ in Eq. (41) is the equivalent force corresponding to the misfit eigenstrain within the QWR.

We assume that the matrix and QWR are perfectly bonded along the interface S, that is, the continuity conditions $\boldsymbol{u}^{(m)}=\boldsymbol{u}^{(w)}$ and $\boldsymbol{t}^{(m)}=-\boldsymbol{t}^{(w)}$ hold. Then the number of unknowns is identical to the number of equations and all the nodal displacements and tractions can be determined. Fur-

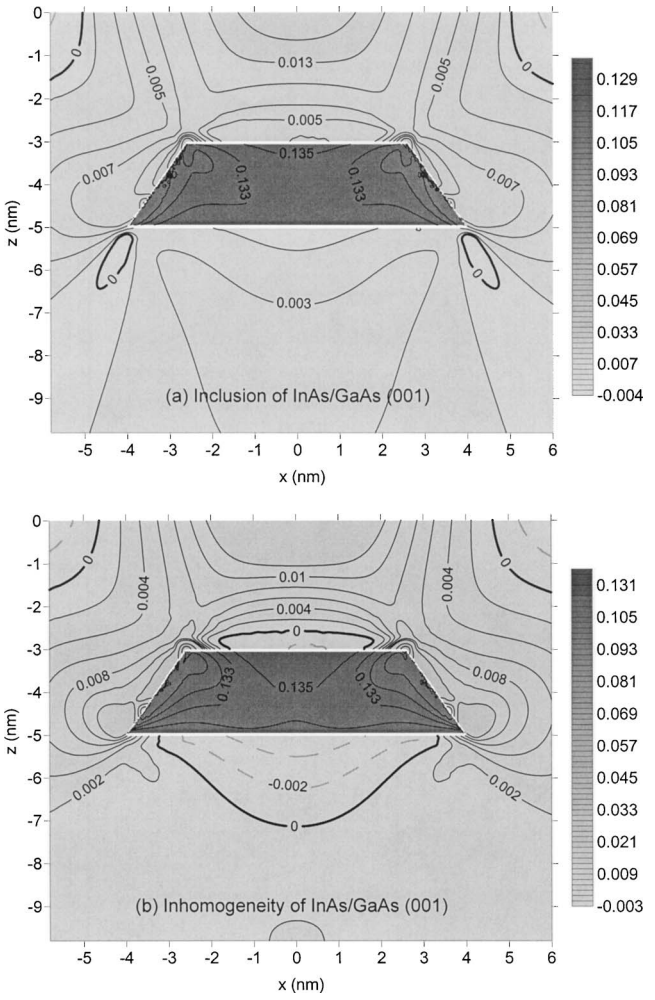

FIG. 5. Contour of hydrostatic strain $(\gamma_{xx}+\gamma_{zz})$ of trapezoid QWR inside GaAs (001) half plane. GaAs (001) inclusion in (a) and InAs (001) inhomogeneity in (b).

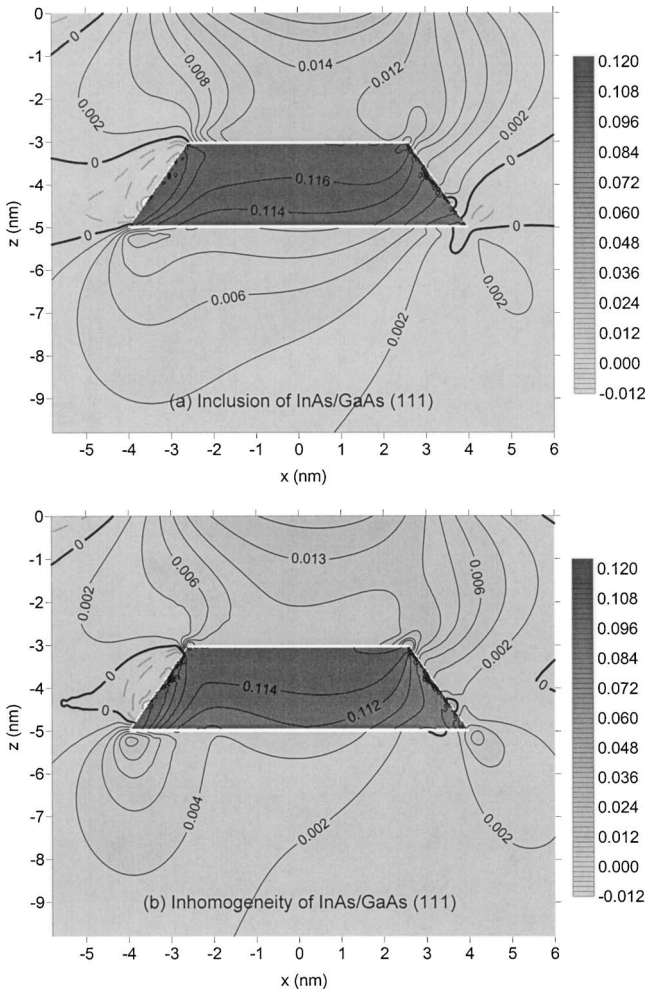

FIG. 6. Contour of hydrostatic strain $(\gamma_{xx}+\gamma_{zz})$ of trapezoid QWR inside GaAs (111) half plane. GaAs (111) inclusion in (a) and InAs (111) inhomogeneity in (b).

thermore, making use of Somigliana's identity, the displacement at any location within either the QWR or the matrix can be easily obtained as

$$b_{ij}u_j = \sum_{n=1}^{N}\left(\int_{\Gamma_n} U_{ij}^{(m,w)}d\Gamma\right)t_{jn} - \sum_{n=1}^{N}\left(\int_{\Gamma_n} U_{ij}^{(m,w)}d\Gamma\right)u_{jn} + \sum_{n=1}^{N}\left(\int_{\Gamma_n} U_{ij}^{(w)}d\Gamma\right)f_{jn}^{(w)}, \tag{43}$$

where the last force term exists for the QWR domain only. Furthermore, utilizing the basic Eqs. (1)–(5), all the internal elastic response in the matrix and QWR can also be calculated.

In summary, we have derived the exact boundary integral equations for the QWR and matrix domains by assuming constant elements along their interface. These equations can be used to find the elastic response along the interface and at any location within the QWR and its surrounding matrix. Before applying our exact closed-form solutions to a buried InAs QWR in GaAs, we have first checked these solutions against available results[26,27] for different QWR inclusions in full-plane/half plane systems and our solutions are found to be the same as previously published results.

VI. NUMERICAL ANALYSIS

In this section, we study the InAs QWRs with two different shapes (square and trapezoid) but with the same cross-section area (13.1716 nm^2) as shown in Fig. 2. Their centroid c has the same coordinate $(0,-4$ nm) and is located symmetrically about the z axis. Same uniform misfit hydrostatic strain is assumed within the QWRs, i.e., $\gamma_{xx}^{*}=\gamma_{yy}^{*}=\gamma_{zz}^{*}=0.07$. In the homogeneous inclusion model, the QWR is assumed to have the same elastic properties as its matrix (i.e., GaAs), while in the complete inhomogeneity model the elastic properties are assumed to be those of the bulk InAs. Two orientations are considered: One is InAs/GaAs (001) in which the global coordinates x, y, and z are coincident with the crystalline axes [100], [010], and [001], and the other is InAs/GaAs (111) where the x axis is along $[11\bar{2}]$, y axis along $[\bar{1}10]$, and z axis along [111] directions of the crystal. The bulk elastic constants of InAs and GaAs for the two different orientations [i.e., (001) and (111)] are given in Appendix B. We further emphasize that the material orientations for both the QWR and its matrix are assumed to be the same

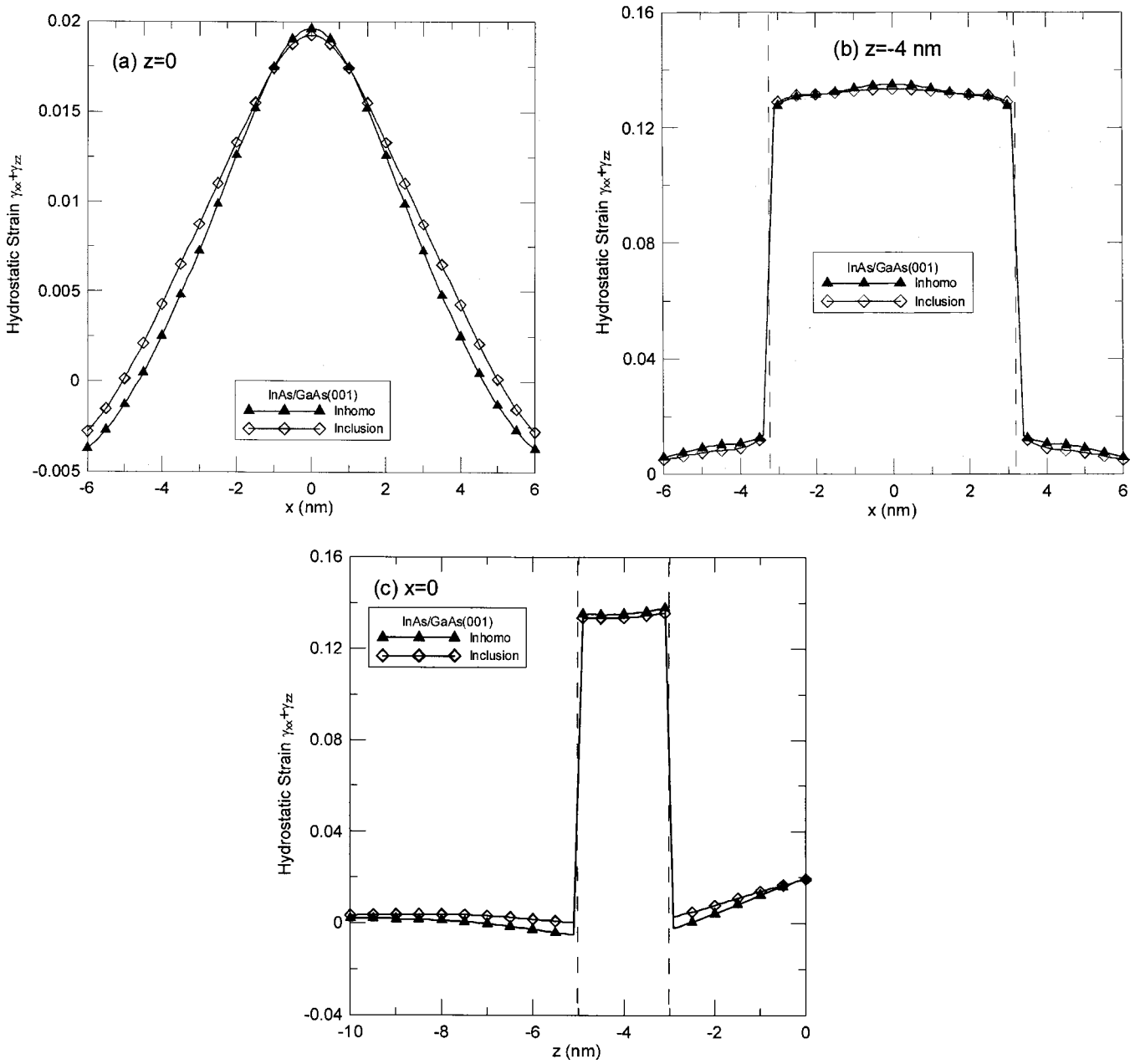

FIG. 7. Variation of hydrostatic strain ($\gamma_{xx}+\gamma_{zz}$) along different straight lines in GaAs (001) half plane with trapezoid QWR inside: GaAs (001) inclusion vs InAs (001) inhomogeneity. (a) Along the x axis ($z=0$). (b) Along the horizontal interior line ($z=-4$ nm). (c) Along the z axis ($x=0$).

in all the numerical examples, and that the boundary condition on the surface of the substrate is assumed to be traction-free.

A. Singular behavior of a square QWR within the infinite substrate

In order to study the singular behavior at the corner, we first apply our BEM solution to a square QWR within the GaAs full plane as shown in Fig. 2(a). Figures 3 and 4 show the corresponding strain field variations along the upper right diagonal line of the square QWR inside GaAs (001) and (111) full planes [dashed line in Fig. 2(a), from point c to c' with its middle point at the upper right vertex; plotted using the horizontal x axis from 0 to 3.6293 nm].

It is observed from the strain curves that for both the GaAs (001) and (111) substrate cases, the shear strain component γ_{xz} is (logarithmically) singular at the corner [Figs. 3(b) and 4(b)]. However, the induced hydrostatic strain, $\gamma_{xx}+\gamma_{zz}$, shows the singular behavior only when the material is in (111) orientation [Fig. 4(a)]. Comparing further Fig. 3 to Fig. 4, we see that the strain values are slightly different for the two different oriented quantum structures, with the maximum difference being within 10%.

For fixed orientation of the nanostructure [either (001) or (111)], we also observed that the hydrostatic strains are comparable for the two different models (inclusion and inhomogeneity) when the field points are far away from the center c. At the center, however, the hydrostatic strain from both models has the maximum difference, with the homogeneous in-

clusion model overestimating the strain by about 10%. On the other hand, in the near exterior of the QWR, the hydrostatic strain predicted in terms of the inhomogeneous model is larger than that based on the inclusion model. For the shear strain in Figs. 3(b) and 4(b), it can be observed that its magnitude in terms of the inhomogeneity is slightly larger inside the QWR and smaller outside the QWR as compared to that obtained from the homogeneous inclusion model.

B. Elastic response of a trapezoid QWR within the half plane substrate

We now assume a more realistic trapezoidal QWR structure model within a half plane substrate, and the effect of the traction-free surface in this situation is considered. As shown in Fig. 2(b), the trapezoidal QWR was chosen to have crystallographically allowed sidewall angles for the (111) orientation so that the length along the top is 5.1716 nm and along the bottom 8 nm. Again, the centroid is located at (0, −4 nm) with a height of 2 nm.

Figures 5 and 6 show the contour of hydrostatic strain inside the half plane with (a) and (b) corresponding to the simplified inclusion and complete inhomogeneity models, respectively. As expected, the strain field is symmetric about the z axis for the (001) structure (Fig. 5) and asymmetric for the (111) orientation (Fig. 6). We further notice that the hydrostatic strain value inside the QWR is much larger than that of the outside, while the concentration near the center of the free surface can be also observed from Figs. 5 and 6. We mark the zero value with a thick line, which is the transition from tensile (positive values plotted as solid lines) to compressive domains (negative values plotted as dashed lines). In general, the differences between models affect the regions inside or nearby, but exterior to, the QWR.

Figures 7 and 8 plot the variation of hydrostatic strain ($\gamma_{xx}+\gamma_{zz}$) along three straight lines in the half plane with a trapezoidal QWR inside: along the surface x axis ($z=0$) in (a), along the horizontal interior line ($z=-4$ nm) in (b), and along the vertical z axis ($x=0$) in (c). The result for the (001) orientation is shown in Fig. 7 and that for the (111) orientation in Fig. 8. It is observed that the strain fields for both models are similar along the surface line [Figs. 7(a) and 8(a)]: In the (001) orientation, the maximum strain occurs at the center, and for the (111) orientation the maximum value occurs on the right-hand side of z axis. From Figs. 7(b), 7(c), 8(b), and 8(c), we also notice that the strain field inside the QWR is much larger than that of the outside, which is consistent with the observations from Figs. 5 and 6. Again, the differences between the model results are very small and can be ignored if the region of interest is not close to the QWR boundary. However, the difference from the two different models can be as large as 10% for points within or close to the QWR.

VII. CONCLUDING REMARKS

In the paper, we proposed an accurate BEM for modeling the strain in quantum nanostructures and applied the technique to a QWR embedded in a substrate. By utilizing half plane Green's functions, their analytic integrals, as well as interface conditions, the elastic response at any location can be predicted based on the inclusion and inhomogeneity models. From our study, some important features are observed.

(1) In the substrate and far away from the QWR, both the inclusion and inhomogeneity models predict very close results. In other words, if one is only interested in the elastic fields far away from the QWR interface, the simplified homogeneous inclusion model can be safely applied.
(2) For points inside or close to the QWR, the difference between the two models can be as high as 10% for the test structures, which can result in strong variations of the confined electronic states.
(3) While the singular behavior near the corners of the QWR looks similar for both inclusion and inhomogeneity models, the amplitudes of the singularities are different.

ACKNOWLEDGMENTS

This work was carried out while one of the authors (E.P.) was associated with the School of Mechanical and Production Engineering at Nanyang Technological University under the Tan Chin Tuan Exchange Fellowship in the summer of 2004. He would like to thank Professor K. M. Liew and the School for their hospitality during his stay there. One of the authors (J.D.A.) was supported in part by AFOSR.

APPENDIX A: STROH EIGENVALUES P_J AND EIGENMATRICES A

The eigenvalue p and eigenvector $\boldsymbol{a}$ appearing in Eq. (13) satisfy the following eigenrelation in the (x,z) plane:

$$[\boldsymbol{Q}+p(\boldsymbol{R}+\boldsymbol{R}^T)+p^2\boldsymbol{T}]\boldsymbol{a}=0, \tag{A1}$$

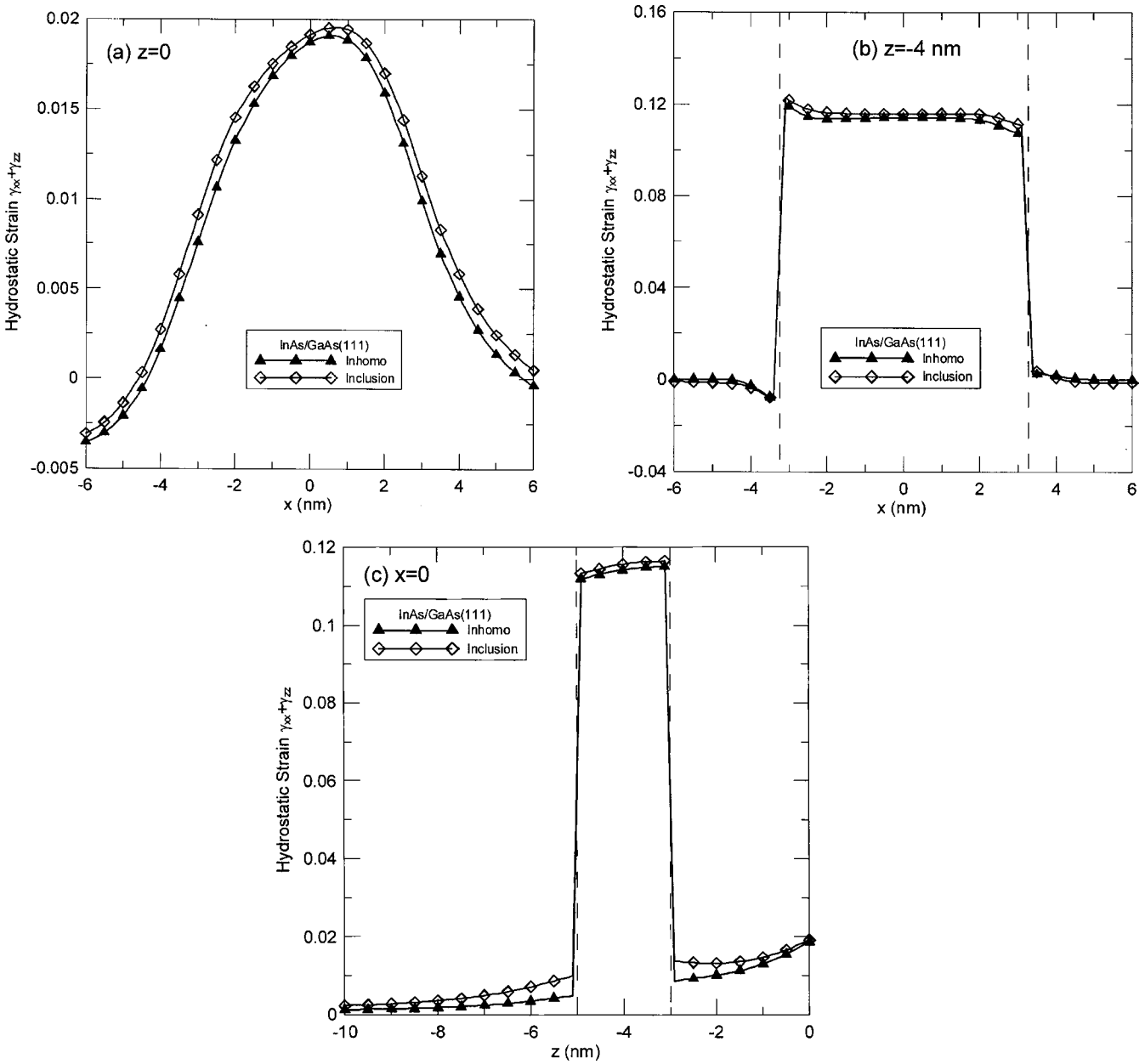

FIG. 8. Variation of hydrostatic strain ($\gamma_{xx}+\gamma_{zz}$) along different straight lines in GaAs (111) half plane with trapezoid QWR inside: GaAs (111) inclusion vs InAs (111) inhomogeneity. (a) Along the x axis (z=0). (b) Along the horizontal interior line (z=−4 nm). (c) Along the z axis (x=0).

where the superscript T denotes matrix transpose, and

$$Q_{ik}=C_{i1k1},\quad R_{ik}=C_{1ik3},\quad T_{ik}=C_{i3k3} \tag{A2}$$

with

$$\boldsymbol{b}=(\boldsymbol{R}^T+p\boldsymbol{T})\boldsymbol{a}=-\frac{1}{p}(\boldsymbol{Q}+p\boldsymbol{R})\boldsymbol{a}. \tag{A3}$$

Denoting by p_m, $\boldsymbol{a}_m$, and $\boldsymbol{b}_m$ ($m=1,2,\ldots,6$) the eigenvalues and the corresponding eigenvectors of Eq. (A1), we can order them in a way so that

$$\begin{aligned}&\mathrm{Im}\,p_j>0,\quad p_{j+3}=\bar{p}_j,\quad \boldsymbol{a}_{j+3}=\bar{\boldsymbol{a}}_j,\quad \boldsymbol{b}_{j+3}=\bar{\boldsymbol{b}}_j,\quad (j=1,2,3),\\ &\boldsymbol{A}=[\boldsymbol{a}_1,\boldsymbol{a}_2,\boldsymbol{a}_3],\end{aligned} \tag{A4}$$

where Im stands for the imaginary part of a complex variable and an overbar for the complex conjugate. We assume that the eigenvalues p_j are distinct and the eigenvectors $\boldsymbol{a}_j$ and $\boldsymbol{b}_j$ satisfy the normalization relation[12]

$$\boldsymbol{b}_i^T\boldsymbol{a}_j + \boldsymbol{a}_i^T\boldsymbol{b}_j = \delta_{ij}, \tag{A5}$$

with δ_{ij} being the 3×3 Kronecker delta, i.e., the 3×3 identity matrix. We also remark that repeated eigenvalues p_j can be avoided by using slightly perturbed material coefficients with negligible errors. In doing so, the simple structure of the solution presented in the text can always be utilized.

APPENDIX B: ELASTIC COEFFICIENTS OF INAS AND GAAS IN (001) AND (111) DIRECTIONS

(1) InAs in (001) direction:

$$[C] = \begin{bmatrix} 83.29 & 45.26 & 45.26 & 0 & 0 & 0 \\ 45.26 & 83.29 & 45.26 & 0 & 0 & 0 \\ 45.26 & 45.26 & 83.29 & 0 & 0 & 0 \\ 0 & 0 & 0 & 39.59 & 0 & 0 \\ 0 & 0 & 0 & 0 & 39.59 & 0 \\ 0 & 0 & 0 & 0 & 0 & 39.59 \end{bmatrix} (10^9\ \mathrm{N/m^2}), \tag{B1}$$

(2) GaAs in (001) direction:

$$[C] = \begin{bmatrix} 118.8 & 53.8 & 53.8 & 0 & 0 & 0 \\ 53.8 & 118.8 & 53.8 & 0 & 0 & 0 \\ 53.8 & 53.8 & 118.8 & 0 & 0 & 0 \\ 0 & 0 & 0 & 59.4 & 0 & 0 \\ 0 & 0 & 0 & 0 & 59.4 & 0 \\ 0 & 0 & 0 & 0 & 0 & 59.4 \end{bmatrix} (10^9\ \mathrm{N/m^2}), \tag{B2}$$

(3) InAs in (111) direction:

$$[C] = \begin{bmatrix} 103.87 & 38.402 & 31.543 & 0 & 9.6991 & 0 \\ 38.402 & 103.87 & 31.543 & 0 & -9.6991 & 0 \\ 31.543 & 31.543 & 110.72 & 0 & 0 & 0 \\ 0 & 0 & 0 & 25.873 & 0 & -9.6991 \\ 9.6991 & -9.6991 & 0 & 0 & 25.873 & 0 \\ 0 & 0 & 0 & -9.6991 & 0 & 32.732 \end{bmatrix} (10^9\ \mathrm{N/m^2}), \tag{B3}$$

(4) GaAs in (111) direction:

$$[C] = \begin{bmatrix} 145.0 & 45.0 & 36.0 & 0 & 12.728 & 0 \\ 45.0 & 145.0 & 36.0 & 0 & -12.728 & 0 \\ 36.0 & 36.0 & 154.0 & 0 & 0 & 0 \\ 0 & 0 & 0 & 41.0 & 0 & -12.728 \\ 12.728 & -12.728 & 0 & 0 & 41.0 & 0 \\ 0 & 0 & 0 & -12.728 & 0 & 50.0 \end{bmatrix} (10^9\ \mathrm{N/m^2}). \tag{B4}$$

[1] M. Grundmann, O. Stier, and D. Bimberg, Phys. Rev. B **52**, 11969 (1995).
[2] L. O. Caro and L. Tapfer, Phys. Rev. B **51**, 4381 (1995).
[3] G. Goldoni, F. Rossi, and E. Molinari, Phys. Status Solidi A **164**, 265 (1997).
[4] G. Goldoni, F. Rossi, and E. Molinari, Physica B **272**, 518 (1999).
[5] D. Bimberg, M. Grundmann, and N. N. Ledentsov, *Quantum Dot Heterostructures* (Wiley, New York, 1998).
[6] A. D. Andreev and E. P. O'Reilly, Phys. Rev. B **62**, 15851 (2000).
[7] E. Pan and B. Yang, J. Appl. Phys. **90**, 6190 (2001).
[8] E. Pan, J. Appl. Phys. **91**, 6379 (2002).
[9] D. A. Faux, J. R. Downes, and E. P. O'Reilly, J. Appl. Phys. **80**, 2515 (1996).
[10] C. Q. Ru, Proc. R. Soc. London, Ser. A **456**, 1051 (2000).
[11] F. Glas, Phys. Status Solidi B **237**, 599 (2003).
[12] T. C. T. Ting, *Anisotropic Elasticity* (Oxford University Press, Oxford, 1996).
[13] T. Mura, *Micromechanics of Defects in Solids*, 2nd ed. (Kluwer, Dordrecht, 1987).
[14] N. Nozaki and M. Taya, J. Appl. Mech. **68**, 441 (2001).
[15] D. A. Faux, J. R. Downes, and E. P. O'Reilly, J. Appl. Phys. **82**, 3754 (1997).
[16] H. Y. Yu, J. Mech. Phys. Solids **49**, 261 (2001).

[17]C. Q. Ru, J. Appl. Mech. **66**, 315 (1999).
[18]X. Wang and Y. P. Shen, Int. J. Eng. Sci. **41**, 85 (2003).
[19]E. Pan, J. Mech. Phys. Solids **52**, 567 (2004).
[20]X. Jiang and E. Pan, Int. J. Solids Struct. **41**, 4361 (2004).
[21]T. Benabbas, P. Francois, Y. Androussi, and A. Lefebvre, J. Appl. Phys. **80**, 2763 (1996).
[22]B. Jogai, J. Appl. Phys. **88**, 5050 (2000).
[23]C. A. Brebbia and J. Dominguez, *Boundary Elements: An Introductory Course* (Computational Mechanics, Southampton, UK, 1992).
[24]B. Yang and E. Pan, J. Appl. Phys. **92**, 3084 (2002).
[25]E. Pan, Proc. R. Soc. London, Ser. A **458**, 181 (2002).
[26]F. Glas, Philos. Mag. A **82**, 2591 (2002).
[27]E. Pan and X. Jiang, Comput. Model. Eng. Sci. **6**, 77 (2004).